Journal of Structural Geology 33 (2011) 1436–1445

Contents lists available at SciVerse ScienceDirect

Journal of Structural Geology

journal homepage: www.elsevier.com/locate/jsg

Subduction related antigorite CPO patterns from forearc mantle in the Sanbagawa belt, southwest Japan

A. Nishii[a,*], S.R. Wallis[a], T. Mizukami[b], K. Michibayashi[c]

[a] Department of Earth and Planetary Sciences, Graduate School of Environmental Studies, Nagoya University, Nagoya 464-8601, Japan
[b] Department of Earth Science, Graduate School of Environmental Studies, Kanazawa University, Kanazawa 920-1192, Japan
[c] Institute of Geosciences, Shizuoka University, Ohya 836, Suruga-ku, Shizuoka 422-8529, Japan

ARTICLE INFO

Article history:
Received 28 April 2011
Received in revised form
25 July 2011
Accepted 11 August 2011
Available online 22 August 2011

Keywords:
Antigorite
Crystallographic preferred orientation
Higashi-Akaishi
Seismic anisotropy

ABSTRACT

Antigorite (Atg) is stable throughout large parts of the wedge mantle of most subduction zones. Atg shows strong acoustic anisotropy and crystallographic preferred orientation (CPO) patterns of this mineral may contribute significantly to seismic anisotropy in convergent margins. Atg CPO patterns from the Higashi-Akaishi (HA) forearc mantle body of southwest Japan adds to the data set suggesting the most common Atg CPO pattern has a c-axis perpendicular to the foliation and a b-axis parallel to the stretching lineation. Statistical analysis using the eigenvector method of Atg CPO from two mutually perpendicular directions in the same sample (*YZ*-section and *XZ*-section) shows no significant differences implying sample preparation has no significant affect on the resulting Atg CPO. Reuss (uniform stress) averages of anisotropy for the Higashi-Akaishi samples are approximately treble the values for Voigt (uniform strain) averages. When comparing calculated anisotropy of hydrated mantle peridotite samples—such as the Higashi-Akaishi unit—with observed S-wave delay times in convergent margins, the appropriate averaging method needs to be considered.

1. Introduction

Thermal modeling and petrological studies suggest that antigorite (Atg) is stable throughout large parts of the wedge mantle of most subduction zones (e.g. Ulmer and Trommsdorff, 1995; Hyndman and Peacock, 2003; Wada et al., 2008). There is also observational evidence for the presence of this mineral in convergent margins, in particular close to the subduction boundary (e.g. Bostock et al., 2002; Blakely et al., 2005; Wada et al., 2008; Kawakatsu and Watada, 2007). Atg has an acoustic anisotropy much stronger than olivine (Ol) (Bezacier et al., 2010)—the major constituent mineral of the mantle wedge—and a number of recent studies have emphasized the possible importance of Atg crystallographic preferred orientations (CPO) in discussing seismic anisotropy in convergent margins (e.g. Katayama et al., 2009; Faccenda et al., 2008). However, only a few examples of natural Atg CPO patterns have been published (Bezacier et al., 2010; Hirauchi et al., 2010; Jung, 2011; Moortèle et al., 2010; Soda and Takagi, 2010). From the limited data available it seems there are two distinct types of Atg CPO. Both types have c-axes concentrated in a direction perpendicular to the foliation, but they differ in whether there is a concentration of a-axes or b-axes parallel to the mineral lineation. We refer to these two distinct types as A- and B-types, respectively. In this contribution we report a further example of a B-type Atg CPO from the Higashi-Akaishi (HA) garnet peridotite body of SW Japan. This body represents a sliver of forearc mantle (Mizukami and Wallis, 2005; Hattori et al., 2010) and the related Atg fabrics formed during subduction (Mizukami and Wallis, 2005). These Atg CPOs, therefore, are likely to be representative of CPO fabrics in the mantle wedge. In this contribution, we discuss the implications of our CPOs for wedge mantle seismic anisotropy. We also address an issue of whether any artifacts are introduced in the CPO due to disruption of the crystal lattice either by small-scale plastic deformation or brittle processes caused during sample preparation. Such disruption need only be on a scale of a few nm to influence the measured CPO. As far as we are aware there has been no systematic study of this issue. If such a problem exited for Atg it could also be a significant issue for other sheet silicates.

2. Geology of the Higashi-Akaishi body

The Higashi-Akaishi (HA) peridotite is part of the oceanic subduction type Sanbagawa metamorphic belt and is located in the Besshi region of central Shikoku, Japan (Fig. 1). The HA body is a sliver of mantle wedge exhumed from depths of 100 km or more

* Corresponding author.
E-mail address: nishii.aya@c.mbox.nagoya-u.ac.jp (A. Nishii). .

0191-8141/$ – see front matter
doi:10.1016/j.jsg.2011.08.006

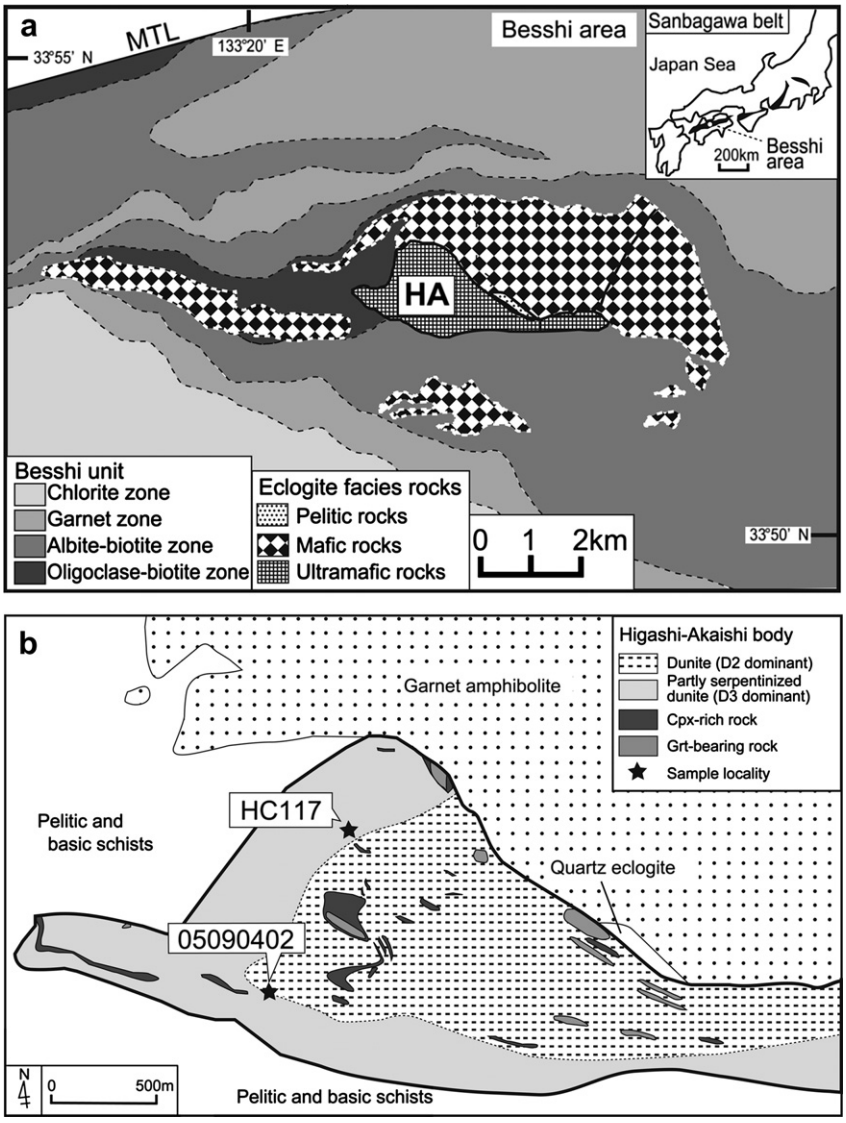

Fig. 1. (a) Geological map of the Besshi area modified after Aoya (2001). Only clearly identified eclogite facies areas are shown and the extent of similar grade rocks is likely to be considerably wider (e.g. Kouketsu and Enami, 2010). HA = Higashi-Akaishi peridotite body; MTL = Median Tectonic Line. (b) Geological map showing the distribution of areas preserving D2 and D3 fabrics and the sample localities.

(Enami et al., 2004; Mizukami and Wallis, 2005). A combination of microstructural and petrological studies allows four distinct deformation phases of high strain ductile deformation (D1–D4) to be identified within the body; the dominant deformation D2 occurred during subduction and the subsequent D3 and D4 stages are related to exhumation (Mizukami and Wallis, 2005). The tectonic significance of D1 is unclear. Antigorite (Atg) first formed during the later part of the D2 deformation. Therefore, we differentiate between the early Atg-free and later Atg-bearing stages and refer to these as D2a and D2b, respectively. A combination of garnet-orthopyroxene geothermobarometry with microstructural observations shows D2a was associated with increasing pressure with a peak in excess of 2.8 GPa and temperatures of 700–800 °C (Mizukami and Wallis, 2005). The increasing pressure shows that D2 formed during subduction. Atg that formed during the D2b stage is parallel to the D2a tectonic fabrics and shows syndeformational microstructures, which are interpreted as part of the same tectonic event as D2a (Wallis et al., in press). D2 took place in the presence of H_2O-rich fluids (Mizukami et al., 2004; Sumino et al., 2010). We suggest the formation of Atg occurred by the reaction of this H_2O with the olivine (Ol) as the temperature of the subduction zone cooled and pressure increased. The extra Si needed to form Atg may have been supplied by clinopyroxene (Cpx) which is present, generally in small quantities, throughout the HA body. The extra Si may also have been supplied by an external fluid. The petrological observations imply an anticlockwise P–T path, which can be interpreted as reflecting the conditions immediately after the onset of subduction (Mizukami and Wallis, 2005; Endo et al., 2009). The importance of these observations is that the Atg we report here formed at the lower parts of the mantle wedge. In other studies, many Atg schist samples either formed close to the surface or their formation conditions are poorly constrained. There is therefore some uncertainty about how well they reflect conditions deep in the wedge.

3. Sample description

The primary goals of this study are to investigate the type of CPO formed by Atg at depth within a subduction zone and to examine its implications for seismic anisotropy of wedge mantle. We studied

two D2 Atg-bearing dunite samples: 05090402 with 21% Atg and HC117 with 42% Atg (Fig. 2). The rest of the rock for both samples is dominantly Ol with much smaller amounts of chromite and Cpx. The shape preferred orientations (SPOs) of Ol and Atg are very similar and can be used to define a mineral elongation direction within a foliation (Wallis et al., in press). The mineral lineation is parallel to the stretching direction defined by boudinaged spinel. The Atg is developed evenly throughout the samples and does not show a strong concentration in particular layers. However, elsewhere in the HA body cm-thick Atg-rich layers are observed. Cpx-rich layers with similar thicknesses are observed in other parts of the HA body that lacks significant amounts of Atg suggesting the cm-scale layers of Atg may have originated as Cpx layers. Thin sections perpendicular to the foliation were prepared for both samples. Sections both parallel and perpendicular to the mineral lineation were examined. Atg crystals are unusually well-formed and large: grains are generally about 1 mm long and in most cases show only minor undulose extinction.

Ol grains contained in D2a dunite that is free of Atg show a clear CPO pattern with a c-axis maximum parallel to the lineation, a b-axis perpendicular to the foliation and an a-axis within the foliation and perpendicular to the lineation (Wallis et al. in press). This CPO has the same characteristics as the B-type Ol CPO from the same area reported by Mizukami et al. (2004) and Muramoto et al. (2011). In contrast, samples with more than 10% syndeformational Atg show much weaker Ol CPO patterns suggesting that the presence of Atg in peridotite tectonites drastically reduces the strength of associated Ol CPO (Wallis et al., in press).

3.1. Atg CPO

Measurement of Atg CPO was carried out at Shizuoka University using EBSD (Electron back-scattered diffraction). We measured CPO in two mutually perpendicular sections from the same sample: the *XZ*-section (normal to foliation and parallel to lineation), and the *YZ*-section (normal to both foliation and lineation). Thin sections were prepared using a series of diamond pastes of decreasing grain-size with a final polish using a grain size of 0.25 microns. Remaining surface damage was then removed by 30 min of chemical polishing using colloidal silica spread on a vibrating table.

A total number of about 150 Atg grains were measured in each section. The samples are relatively homogenous as shown in Fig. 2. For the measurements we moved the stage a fixed amount and measured the nearest antigorite grain. We also excluded some grains that were clearly secondary and forming along cracks in olivine. The Kikuchi patterns used to determine crystal orientations of Atg grains fade rapidly during measurement—presumably due to beam damage of the crystal structure—so it is necessary to capture an image soon after the beam is directed at a new measurement spot. The results of the CPO measurements are shown in Fig. 3. The results for both samples show a strong concentration of c-axes at a high angle to the foliation and a strong alignment of b-axes parallel to the mineral lineation in all sections. The strength of the fabrics is greater for the sample with more Atg. CPO patterns for Atg a, b, and c crystallographic axes show point concentrations that are significantly different from random at the 99% confidence level (Fig. 4) with the sole exception of the a-axis distribution in the section perpendicular to the stretching lineation for sample 05090402.

4. Sample preparation and the reliability of Atg CPO measurements

Atg is relatively easy to deform and at low P and T semi-brittle processes seem to dominate (e.g. Escartín and Hirth, 1997; Hilairet et al., 2007; Chernak and Hirth, 2010). Because of these characteristics, it is possible that original orientations of the Atg crystals in the rock may be affected by mechanical damage to the surface of the Atg crystals during sample preparation. EBSD patterns reflect the outer most 10 nm (Prior et al., 1999) and even a thin disrupted layer on the surface of the grain could potentially influence the acquired CPO.

To investigate this possibility and to improve our knowledge of Atg CPO, we compared the results from two thin sections made from two perpendicular directions. Any secondary shearing induced by polishing is likely to be affected by the presence of a strong foliation and the crystal structure of Atg. We focused on three possible effects.

1) Perpendicular to the foliation, the Atg grains are in contact with olivine. Support at the grain boundaries will restrict the amount of secondary shearing perpendicular to the foliation. Shearing is therefore likely to be easier parallel to the foliation and any secondary effects should lead to the development of girdles or small circle distributions parallel to the foliation.
2) If mechanical damage is introduced then this should increase as the proportion of weak Atg increases and that of strong Ol decreases.
3) Atg has a curved plate-like crystal form with the fold axis parallel to the crystallographic b-axis. For both A- and B-type CPO with one axis strongly aligned parallel to the stretching direction, different bonds will have to be broken to cause shearing in sections perpendicular and parallel to lineation. The affects on the CPO are therefore likely to be different in the two sections.

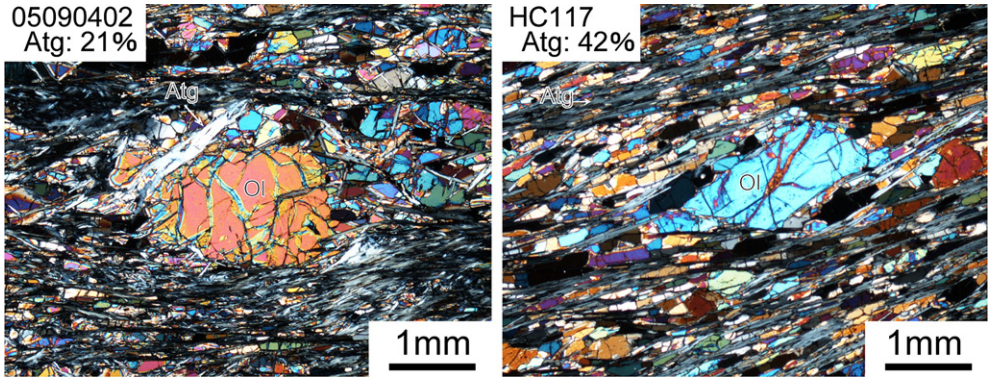

Fig. 2. Photomicrographs showing characteristic microstructures of samples 05090402 (21 modal % Atg) and HC117 (42 modal % Atg).

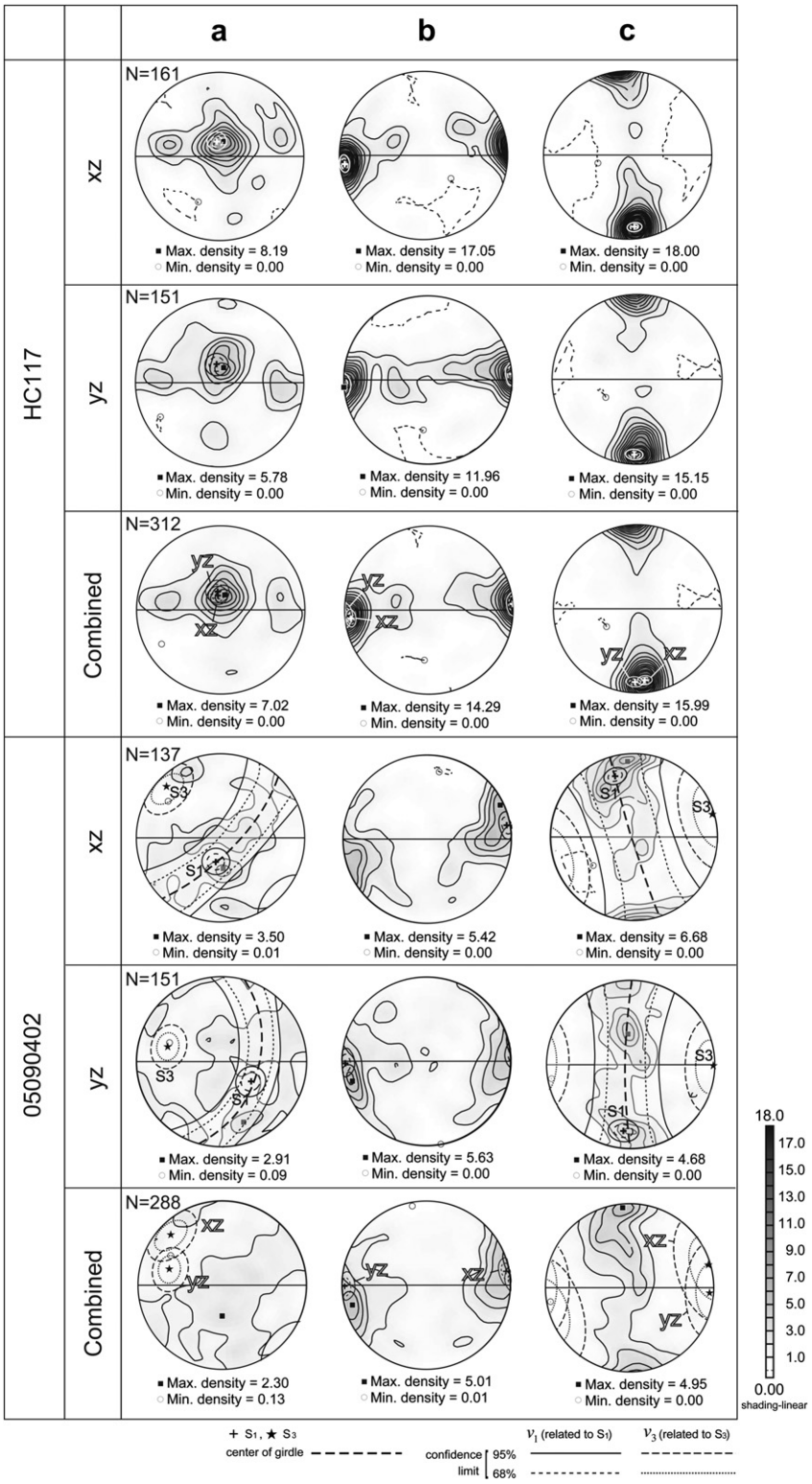

Fig. 3. Atg CPO pattern using an equal area, lower-hemisphere projection with the contours shown as multiples of uniform distribution plotted using software of D. Mainprice. The stretching direction is oriented E–W and the foliation is vertical. The *XZ*-section is normal to the foliation and parallel to the lineation; the *YZ*-section is normal to both the foliation and lineation. The + symbol shows the orientation of ν_1 associated with S_1; the star symbol shows the orientation of ν_3 associated with S_3. The girdle area corresponding the estimate for ν_3 associated with S_3 is shown for the a- and c-axes of sample 05090402. The maximum and minimum concentrations are shown by black squares and open circles, respectively.

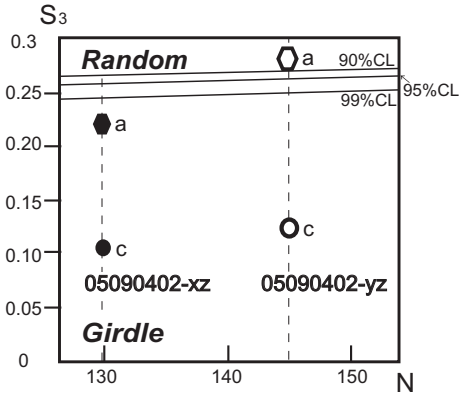

Fig. 4. Critical values for the randomness test of Anderson and Stephens (1972) for different numbers of data points. The vertical axis shows the value of S_3 and the horizontal axis shows the numbers of data points.

To examine the possibility that sample preparation caused secondary artifacts to be introduced in the final CPO, we concentrated on looking for significant differences in the concentration and in distribution of Atg axes in CPO measured for two perpendicular sections from the same sample and between two samples with different amounts of Atg. The significance of any differences can be tested by using statistical analysis of CPO patterns for the two different directions. A suitable method for this type of analysis is the eigenvector analysis of an orientation matrix. This method is briefly described below.

5. Statistical analysis

5.1. Eigenvalue method

Each of the orientation data can be treated as unit vectors with direction cosines l, m, n parallel to three perpendicular axes x, y, z. The data are non-polar and therefore have a rotational symmetry. For relatively simple distributions—such as point concentrations and girdles, which are sufficient for the present study—the main properties of the distribution can be described by comparing the variation of the data from mean values. There are three sets of direction cosine data and three means. A variance can also be defined for each sample. Covariance expresses the distribution of two variables with respect to their means and is defined as

$$\mathrm{cov}(x,y) = \frac{\sum_{i=1}^{N}(X_i-\overline{X})(Y_i-\overline{Y})}{N} \tag{1}$$

In our case there are three orientation variables (l, m, n), and a full range of 9 covariance values can be defined, including the variance of one variable with respect to its own mean. These covariances can be expressed in the covariance matrix:

$$A = \begin{pmatrix} \mathrm{cov}(x,x) & \mathrm{cov}(x,y) & \mathrm{cov}(x,z) \\ \mathrm{cov}(y,x) & \mathrm{cov}(y,y) & \mathrm{cov}(y,z) \\ \mathrm{cov}(z,x) & \mathrm{cov}(z,y) & \mathrm{cov}(z,z) \end{pmatrix} \tag{2}$$

From the definition of covariance it is clear that the matrix is symmetrical and only six of these terms are independent. In addition, the non-polarity of the data and consequent rotational symmetry gives mean values of x, y and z of zero. The resulting matrix can, therefore, be expressed in terms of the direction cosines l, m and n:

$$\frac{1}{N}\begin{pmatrix} \sum l_i^2 & \sum l_i m_i & \sum l_i n_i \\ \sum m_i l_i & \sum m_i^2 & \sum m_i n_i \\ \sum n_i l_i & \sum n_i m_i & \sum n_i^2 \end{pmatrix} \tag{3}$$

(e.g. Woodcock, 1977; Woodcock and Naylor, 1983).

Due to the symmetry of this matrix, its eigenvectors (ν_1, ν_2, ν_3) are mutually perpendicular with the largest vector parallel to the mean direction, the smallest vector perpendicular to any girdle present in the data and the intermediate vector perpendicular to both. The shape of the distribution is shown by the eigenvalues, S_1, S_2 and S_3. The proportions of eigenvalues give information on the nature of the CPO distribution. If the magnitude is $S_1 > S_2 \cong S_3$, it represents a cluster distribution. And in the case of $S_1 \cong S_2 > S_3$, there is a girdle distribution. The values of S_i can also be used for statistical analysis.

5.2. Estimation of error angle

To compare two means from different CPO patterns we need to estimate suitable confidence limits (CL) for estimates of the means. Fisher (1953) devised a factor K (Fisher's constant), which is a measure of clustering. K can be estimated as below (Priest, 1985)

$$K = \frac{1-N^{-1}}{1-NS}. \tag{4}$$

where S refers to the eigenvalue and N to the sample size or number of measurements. The appropriate CL for the mean orientation can be expressed as an angle, θ, which is given by (Priest, 1985)

$$\cos\theta \cong 1 + \frac{\ln(1-P)}{KNS}, \tag{5}$$

where P refers to the probability. For 95% CL the value of P is set at 0.95. So θ for 68% CL is given by

$$\theta = \arccos\left[1 + \frac{\ln(1-0.68)}{KNS}\right] \tag{6}$$

where θ is the angle measured from the mean value. We have plotted the 68% and 95% CL cones with an apical angle corresponding to the values of θ given by (6) (Fig. 3).

6. Comparison of CPO patterns in mutually perpendicular sections

6.1. Statistical analysis

Using the above equations we are now in a position to test the equivalence of the CPO measured for different orientations of the same sample. The results of Atg CPO measurement from two directions are shown in Fig. 3. We use the principal axes of finite strain, X, Y and Z to discuss these sections where X is assumed to be parallel to the mineral lineation and Z is assumed to be perpendicular to the foliation. For the results from the YZ-section, the CPO is shown after a rotation by 90°, so it is in the same reference frame as the CPO for the XZ-section.

Results for HC117 show strong concentrations of the b-axes parallel to the stretching direction, the c-axes perpendicular to the foliation and the a-axes within the foliation and perpendicular to the stretching direction. Confidence limits for the estimates of the mean in the two sections for HC117 were derived using the method described above (Fig. 3). It can be seen that the two sections show no significant difference in the locations of all point maxima for the three crystallographic axes. Both sections have high S_1 values 0.63–0.81 for the XZ-section and 0.53–0.76 for the YZ-section (Table 1).

Table 1
Eigenvalues (S_1, S_2 and S_3), eigenvector (v_1) and confidence levels for each sample. The eigenvectors are given as direction cosines parallel to three perpendicular axes x, y, z. N = number of analyses; CL = Confidence Limit given in degrees.

Sample/axis	N	S_1	S_2	S_3	Eigenvector (v1)	68% CL	95% CL
HC117-xz/a	155	0.63	0.23	0.15	0.075	5	9
					0.24		
					−0.97		
HC117-xz/b	155	0.76	0.19	0.044	−0.99	4	6
					−0.10		
					−0.10		
HC117-xz/c	155	0.81	0.18	0.013	−0.12	3	6
					0.96		
					0.25		
HC117-yz/a	144	0.53	0.29	0.18	−0.95	7	11
					−0.31		
					0.044		
HC117-yz/b	144	0.66	0.28	0.053	−0.0089	5	8
					−0.074		
					−1.00		
HC117-yz/c	144	0.76	0.19	0.050	0.22	4	7
					−0.98		
					0.026		
05090402-xz/a	130	0.47	0.31	0.22	0.060	8	13
					0.40		
					0.92		
05090402-xz/b	130	0.61	0.27	0.12	−0.98	6	10
					−0.18		
					0.076		
05090402-xz/c	130	0.63	0.26	0.10	0.27	6	9
					−0.87		
					0.41		
05090402-yz/a	145	0.40	0.33	0.27	−0.82	9	15
					−0.31		
					−0.48		
05090402-yz/b	145	0.57	0.23	0.21	0.070	6	10
					0.041		
					−1.0		
05090402-yz/c	145	0.46	0.41	0.12	−0.38	8	13
					0.92		
					0.075		

The CPO patterns for 05090402 are weaker than for HC117 (Table 1). Nevertheless, the b-axes show strong concentrations parallel to the stretching direction similar to HC117. In contrast, the c-axes in both sections show a girdle distribution perpendicular to the foliation. The two sections show distinct localized concentrations within this girdle. The a-axes show a broad distribution without any well-defined girdle or point concentration (Fig. 4). For this sample we restrict our discussions to the b- and c-axis CPO. Eigenvector analysis shows that the locations of the b-axis concentrations in the sections are not statistically significantly different. The c-axes maxima for the two sections do not coincide within error. However, the S_3 values show both CPOs can be described as a girdle distribution with S_3 as a pole (Fig. 4). To investigate if these girdles coincide, the confidence limits for the orientation of v_3 were estimated (Fig. 3). For the two samples the CL ranges for v_3 coincide within error and the two S_1 maxima plot within the girdle regions. We conclude, therefore, there is no significant difference between the two CPOs.

6.2. Effect of sample preparation on CPO

As outlined above, secondary shear due to sample preparation is expected to show some or all of the following characteristics:

1) girdle distributions parallel to the foliation;
2) weaker Atg CPO in samples with greater proportions of Atg; and
3) different development of CPO patterns in sections parallel and perpendicular to b-axis maxima.

Our samples show none of these characteristics implying that sample preparation has no significant affect on the measured Atg CPO pattern. One of the implications of this result is that the results from the two sections can be combined to estimate to obtain an improved estimate of the Atg CPO for each sample.

6.3. Comparison with other reports

The grain shape of antigorite is closely controlled by its crystallographic orientation and all antigorite CPO patterns from foliated serpentinites show a strong concentration of c-axes at a high angle to the foliation. Natural examples are given by Hirauchi et al. (2010), Jung (2011), Moortèle et al. (2010) and Soda and Takagi (2010) and similar features are seen in experimental samples (Katayama et al., 2009). Some of these examples show a clear point concentration perpendicular to the foliation (Hirauchi et al., 2010; Moortèle et al., 2010) whereas others show a girdle distribution of the c-axes perpendicular to the maximum elongation direction (this study; Soda and Takagi, 2010). Vibrations parallel to the c-axis are the slowest and so the presence of a girdle distribution perpendicular to the stretching direction, L, results in fast seismic wave propagation parallel to L. The clearest girdle distribution is shown by the sample documented in Soda and Takagi (2010) and we have used their orignal data to calculate the seismic properties of the sample (Fig. 5). Point maxima are associated with fast seismic propagation parallel to the foliation without any clear relationship to L. The work of Hirauchi et al. (2010), Katayama et al. (2009) and the present study show that there is a change from girdle distributions to point maxima of c-axes with increasing strain.

A major distinguishing feature between the different antigorite CPO patterns is the relationships between the b- and a-axes and the maximum stretching direction, L. Several natural examples show a clear concentration of b-axes parallel to L—B-type CPO (this study, Hirauchi et al., 2010; Soda and Takagi, 2010). The formation of this type of CPO is understandable if there is slip parallel to the fold axes of the antigorite flexed crystal morphology. However, other studies show a clear concentration of the a-axes parallel to L—A-type CPO (Katayama et al., 2009; Moortèle et al., 2010). There is also a third A—B-type Atg CPO pattern where the a- and b-axes lie distributed within the foliation (e.g. Jung, 2011). The reasons for the formation of these different types of patterns is unclear but is presumably linked to the formation conditions. Seismic properties parallel to the a- and b-axes of antigorite are very similar and so the degree to which the a- and b-axes are aligned parallel to L has little effect on the predicted seismic properties.

To facilitate a comparison with previous studies in Fig. 5, we used composite Atg CPO patterns made by combining data from the two different directions for both samples. These composite CPO patterns (Fig. 3) were then used to calculate the seismic anisotropy (Fig. 5). These diagrams are oriented with the stretching direction horizontal and the foliation perpendicular. The samples consist almost entirely of antigorite and olivine. The olivine grains for each sample only have a weak CPO pattern (Wallis et al., in press) and the effect of including these grains in our calculations is mainly to reduce the degree of anisotropy. There is also a slight increase in the maximum P wave velocity. These results are comparable to those of Jung (2011).

6.4. Seismic anisotropy associated with Atg CPO in the Higashi-Akaishi unit

Atg has a strong acoustic anisotropy (Bezacier et al., 2010), and Atg CPO may make an important contribution to the seismic anisotropy of mantle wedge material particularly close to the

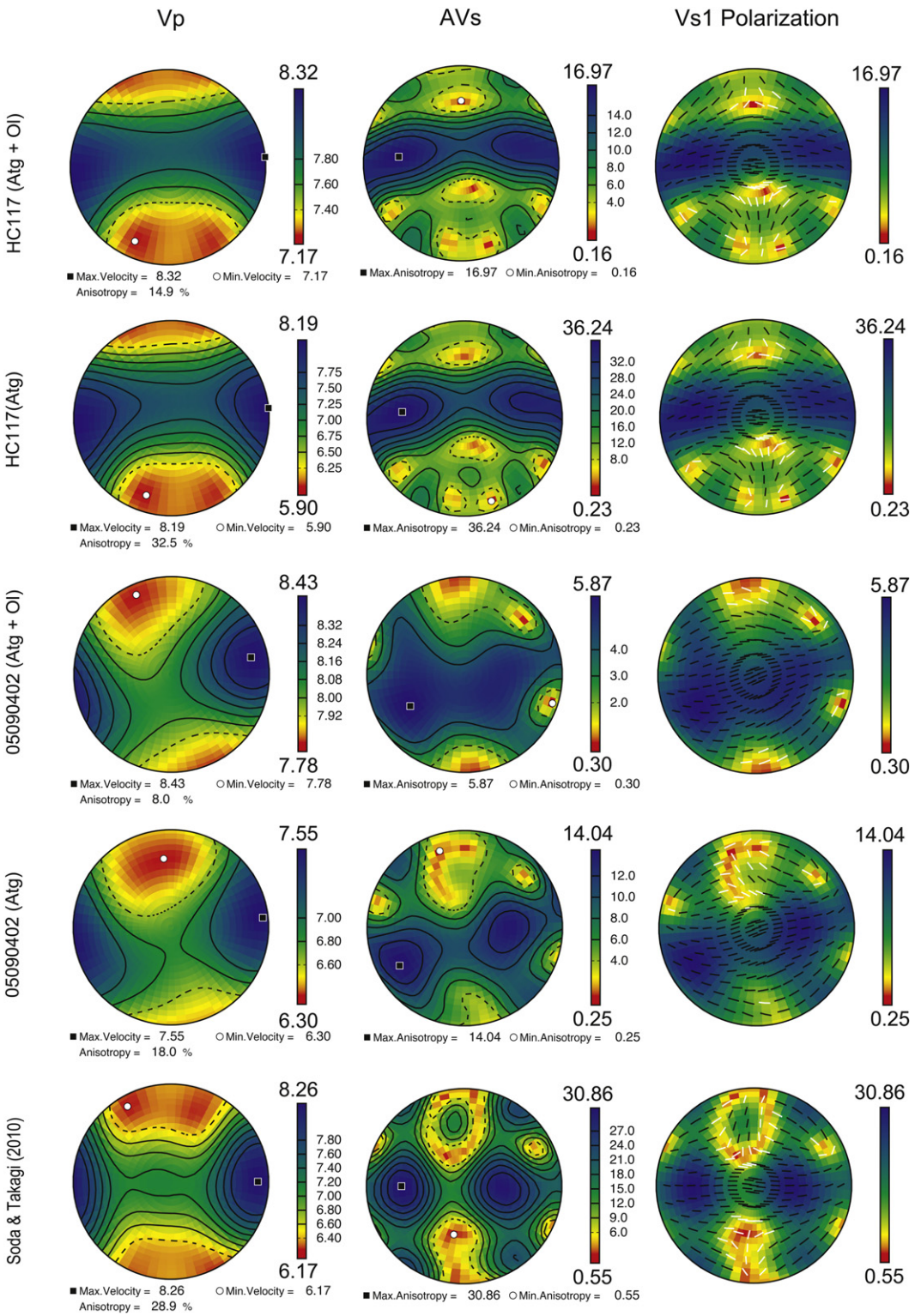

Fig. 5. Atg anisotropies calculated for HC117, 05090402 and the CPO reported by Soda and Takagi (2010) using software of D. Mainprice. The original U-stage measurements for Soda and Takagi (2010) were supplied by Y. Soda and converted to Euler angles using software developed as part of the study by Wallis et al. (in press) and available from the following URL http://web.me.com/westerngate/pubs.html.

subducting slab, where Atg is thought to be widespread. The anisotropy recognized in our samples can be compared to the delay times recognized for S-wave splitting in convergent margins. The delay time is a function of the strength of anisotropy of the medium the S-waves pass through and its thickness (e.g. Silver, 1996). The relationship between anisotropy and maximum delay time is given by:

$$\frac{dt}{L} = \frac{AVs}{\langle Vs \rangle} \tag{7}$$

where dt is the delay time of shear waves, *AVs* is the anisotropy for a specific propagation direction, $<Vs>$ is the average velocity of the fast and slow velocities, and L is the thickness of the anisotropic layer.

To calculate seismic anisotropy from the CPO, some assumption about the interaction between grains within the sample is required. Two extremes are to assume stress constant (Reuss average) and strain constant (Voigt average) behavior. The Reuss average represents unconnected grains free to deform in response to a uniform stress imposed by a surrounding homogenous matrix. In contrast, the Voigt average is appropriate for samples where there is a network of grains that respond to externally imposed kinematics. It is generally assumed that in nature some intermediate state will be achieved and the average of the two types of behavior is used. For minerals such as olivine, the difference between Voigt and Reuss averages is small. However, for more anisotropic minerals, such as Atg, the difference is large and some consideration of whether a simple average is appropriate is required.

The choice of an appropriate value for the anisotropy depends on the orientation of the CPO with respect to the applied force (e.g. Bunge, 1985), or in the present case, the propagation path of the seismic wave with respect to the CPO. When the Atg foliation is at a high angle to the seismic path, then the anisotropy will be best approximated by Voigt average, because the grains will be moving in directions where they are already in contact. In contrast, when the wave propagation is at a low angle to the Atg foliation the average will be better represented by the Reuss average.

We calculated the anisotropy for our samples using both Voigt and Reuss averages (Fig. 6). For these calculations we used not only the Atg measurements presented in this study, but also the olivine data reported in Wallis et al. (in press) for the same samples. The maximum delay times associated with different thicknesses of a layer of mantle with the same CPOs and mineral proportions as the samples described in this contribution were calculated using both Reuss and Voigt averages. For sample HC117, the thickness estimated using Voigt averages is about three times greater than that calculated using Reuss averages. Previous studies report the seismic properties of Atg tectonites use the Voigt–Reuss–Hill average which is the arithmetic mean of the Voigt and Reuss values (e.g. Bezacier et al., 2010; Hirauchi et al., 2010). Our results show this approach can in some circumstances lead to erroneous conclusions and the appropriate average needs to be considered when discussing the relationship between Atg CPO and shear wave time delay.

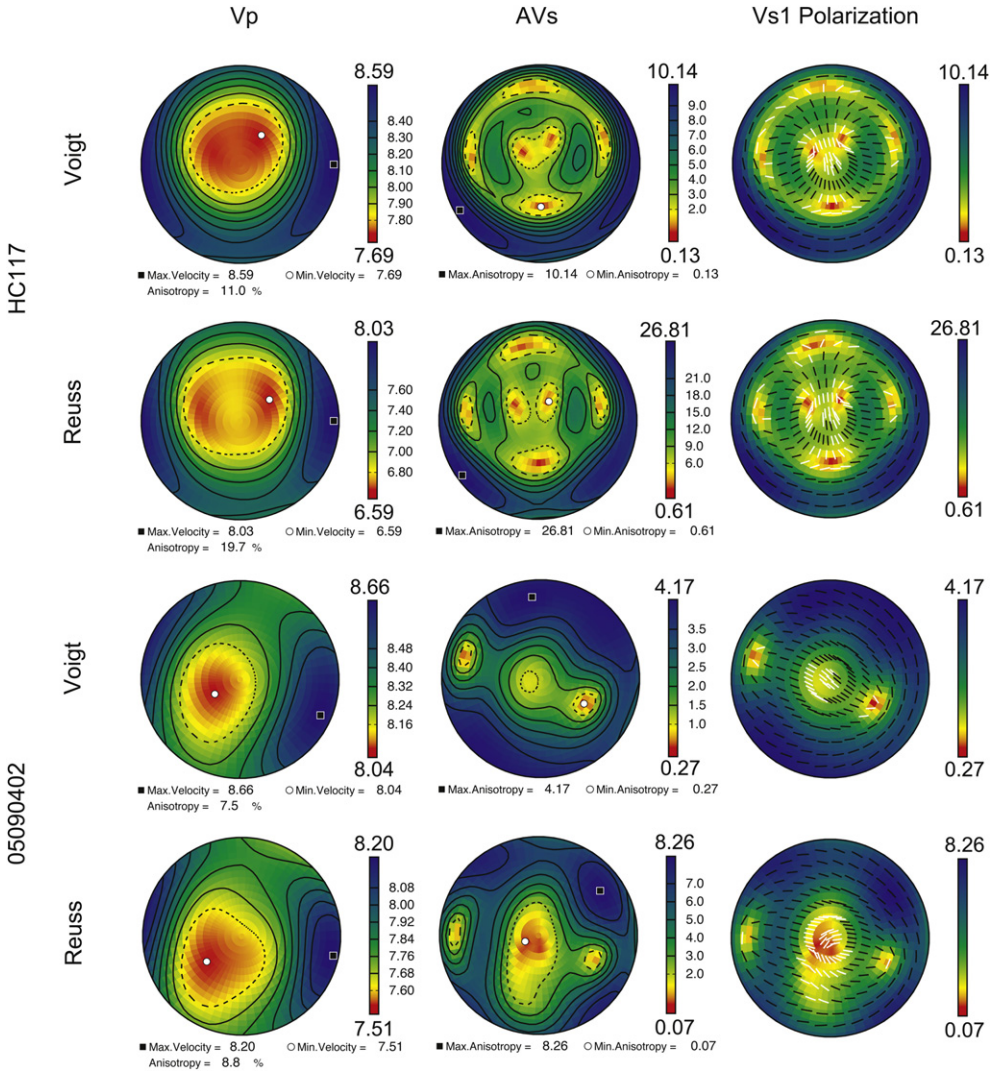

Fig. 6. Atg anisotropies calculated for both samples with Voigt and Reuss. The maximum and minimum anisotropies are shown by black squares and open circles. The ratios of maximum values for the Reuss (R_{max}) and Voigt (V_{max}) averages depend on the amount of Atg: for HC117, $R_{max}/V_{max} = 2.6$ and for 05090402, $R_{max}/V_{max} = 2.0$. The figures are oriented looking down on the foliation with the stretching lineation E–W.

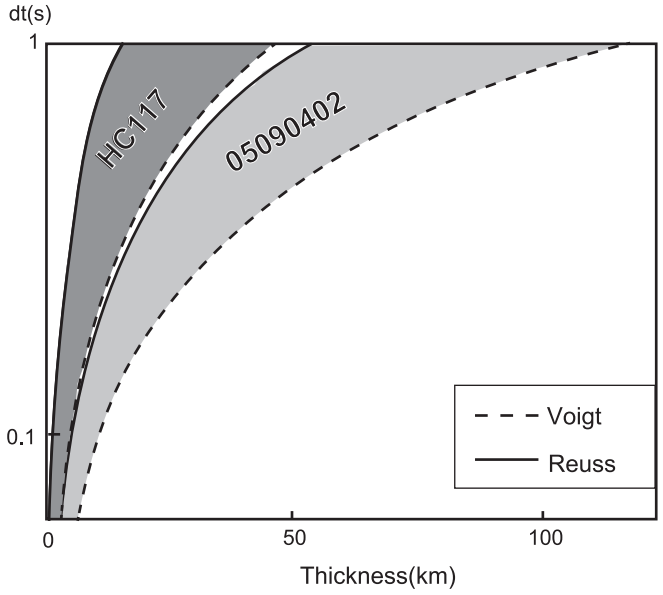

Fig. 7. Relationship between shear wave delay time and the anisotropic layer thickness using values calculated for the hydrated peridotite samples studied in this work and two different assumptions about grain interaction.

Delay times in convergent margins fall in the range of 0.1–1 s (e.g. Nakajima and Hasegawa, 2004; Currie et al., 2004). The calculations presented in Fig. 7 show two important features, 1) There is a significant difference in the estimates of thicknesses required to account for the delay times depending on whether a Voigt or Reuss average is assumed. 2) For the Reuss estimate even the largest delay time can be accounted for by the presence of a layer of Atg-bearing peridotite similar to the Higashi-Akaishi unit that is no more than 5 km thick. Hilairet and Reynard (2009) suggest that serpentinized layers in subduction zones will in general have low thicknesses. Belts of hydrated peridotite, such as the Higashi-Akaishi unit, are, therefore, likely to be common, but may be difficult to recognize using present seismic methods.

7. Conclusions

From our study we can draw the following conclusions about Atg CPO development.

1) The Higashi-Akaishi body shows strong B-type Atg CPO with b-axes parallel to stretching direction. The Atg CPO reported here add to the data set suggesting that B-type Atg patterns are more common than CPO patterns with a-axes parallel to the stretching direction. The deep origin of the Atg of this study suggest B-type Atg CPO patterns are likely to be characteristic of wedge mantle in convergent margins.
2) Atg CPO patterns in sections parallel and perpendicular to the stretching direction show no significant differences, suggesting that sample preparation has no significant affect on the final measured CPO.
3) Calculation of time delay associated with Atg CPO depends strongly on the assumptions about grain interactions: both Reuss and Voigt models should be considered depending on the orientation of the Atg CPO and ray path.

Acknowledgments

We are grateful to M. Enami and T. Watanabe for comments on this work. We are also grateful to H. Kobayashi and other members of the petrology group of Nagoya University for their discussion and encouragement. We also express our appreciation to the graduate students of the Michibayashi laboratory of Shizuoka University for their help with CPO measurement and we are grateful to Dr. Hirauchi, Dr. Soda and Prof. Passchier for their valuable comments on the original manuscript.

References

Anderson, T.W., Stephens, M.A., 1972. Tests for randomness of directions against equatorial and bimodal alternatives. Biometrika 59, 613–621.
Aoya, M., 2001. P-T-D path of eclogite from the Sambagawa belt deduced from combination of petrological and microstructural analysis. Journal of Metamorphic Geology 42, 1225–1248.
Bezacier, L., Reynard, B., Bass, J., Sanchez-Valle, C., Moortèle, B., 2010. Elasticity of antigorite, seismic detection of serpentinites, and anisotropy in subduction zones. Earth and Planetary Science Letters 289, 198–208.
Blakely, R.J., Brocher, T.M., Wells, R.E., 2005. Subduction-zone magnetic anomalies and implications for hydrated forearc mantle. Geology 33, 445–448.
Bostock, M.G., Hyndman, R.D., Rondenay, S., Peacock, S.M., 2002. An inverted continental Moho and serpentinization of the forearc mantle. Nature 417, 536–538.
Bunge, H.J., 1985. Physical properties of polycrystals. In: Wenk, H.-R. (Ed.), Preferred Orientation in Deformed Metals and Rocks. Academic Press, Orlando, USA, pp. 507–525.
Chernak, L.J., Hirth, G., 2010. Deformation of antigorite serpentine at high temperature and pressure. Earth and Planetary Science Letters 296, 23–33.
Currie, C.A., Cassidy, J.F., Hyndman, R.D., Bostock, M.G., 2004. Shear wave anisotropy beneath the Cascadia subduction zone and western North American craton. Geophysical Journal International 157, 341–353.
Enami, M., Mizukami, T., Yokoyama, K., 2004. Metamorphic evolution of garnet-bearing ultramafic rocks from the Gongen area, Sanbagawa belt, Japan. Journal of Metamorphic Geology 22, 1–15.
Endo, S., Wallis, S.R., Hirata, T., Anczkiewicz, R., Platt, J.P., Thirlwall, M., Asahara, Y., 2009. Age and early metamorphic history of the Sanbagawa belt: Lu–Hf and P–T constraints from the Western Iratsu eclogite. Journal of Metamorphic Geology 27, 371–384.
Escartín, J., Hirth, G., 1997. Nondilatant brittle deformation of serpentinites: implications for Mohr-Coulomb theory and the strength of faults. Journal of Geophysical Research 102, 2897–2913.
Faccenda, M., Burlini, L., Gerya, T.V., Mainprice, D., 2008. Fault-induced seismic anisotropy by hydration in subducting oceanic plates. Nature 455, 1097–1100.
Fisher, R.A., 1953. Dispersion on a sphere. Proceedings of the Royal Society of London. Series A, Mathematical and Physical Sciences 217, 295–305.
Hattori, K., Wallis, S., Enami, M., Mizukami, T., 2010. Subduction of mantle wedge peridotites: evidence from the Higashi-akaishi ultramafic body in the Sanbagawa metamorphic belt. Island Arc 19, 192–207.
Hilairet, N., Reynard, B., Wang, Y., Daniel, I., Merkel, S., Nishiyama, N., Petitgirard, Sylvain, 2007. High-pressure creep of serpentine, interseismic deformation, and initiation of subduction. Science 318, 1910–1913.
Hilairet, N., Reynard, B., 2009. Stability and dynamics of serpentinite layer in subduction zone. Tectonophysics 465, 24–29.
Hirauchi, K., Michibayashi, K., Ueda, H., Katayama, I., 2010. Spatial variations in antigorite fabric across a serpentinite subduction channel: Insights from the Ohmachi Seamount, Izu-Bonin frontal arc. Earth and Planetary Science Letters 299, 196–206.
Hyndman, R.D., Peacock, S.M., 2003. Serpentinization of the forearc mantle. Earth and Planetary Science Letters 212, 417–432.
Jung, H., 2011. Seismic anisotropy produced by serpentine in mantle wedge. Earth and Planetary Science Letters. doi:10.1016/j.epsl.2011.05.041.
Katayama, I., Hirauchi, K., Michibayashi, K., Ando, J., 2009. Trench-parallel anisotropy produced by serpentine deformation in the hydrated mantle wedge. Nature 461, 1114–1118.
Kawakatsu, H., Watada, S., 2007. Seismic evidence for deep-water transportation in the mantle. Science 316, 1468–1471.
Kouketsu, Y., Enami, M., 2010. Aragonite and omphacite-bearing metapelite from Besshi region, Sambagawa belt in central Shikoku, Japan and its implication. Island Arc 19, 165–176.
Mizukami, T., Wallis, S.R., Yamamoto, J., 2004. Natural examples of olivine lattice preferred orientation patterns with a flow-normal a-axis maximum. Nature 427, 432–436.
Mizukami, T., Wallis, S., 2005. Structural and petrological constrains on the tectonic evolution of the garnet-lherzolite facies Higashi-akaishi peridotite body, Sanbagawa belt, SW Japan. Tectonics 24, TC6012.
Moortèle, B., Bezacier, L., Trullenque, G., Reynard, B., 2010. Electron back-scattering diffraction (EBSD) measurements of antigorite lattice-preferred orientations (LPO). Journal of Microscopy 239, 245–248.
Muramoto, M., Michibayashi, K., Ando, J., Kagi, H., 2011. Rheological contrast between garnet and clinopyroxene in the mantle wedge: an example from Higashi-akaishi peridotite mass, SW Japan. Physics of the Earth and Planetary Interiors 84, 14–33.
Nakajima, J., Hasegawa, A., 2004. Shear-wave polarization anisotropy and subduction-induced flow in the mantle wedge of northeastern Japan. Earth and Planetary Science Letters 225, 365–377.

Priest, S.D., 1985. Hemispherical Projection Methods in Rock Mechanics. George Allen & Unwin Ltd, London. 39–50.
Prior, D.J., Boyle, A.P., Brenker, F., Cheadle, M.C., Day, A., Lopez, G., Peruzzo, L., Potts, G.J., Reddy, S., Spiess, R., Timms, N.E., Trimby, P., Wheeler, J., Zetterström, L., 1999. The application of electron backscatter diffraction and orientation contrast imaging in the SEM to textural problems in rocks. American Mineralogist 84, 1741–1759.
Silver, P.G., 1996. Seismic anisotropy beneath the continents: Probing the depths of geology. Annual Review of Earth and Planetary Sciences 24, 385–432.
Soda, Y., Takagi, H., 2010. Sequential deformation from serpentinite mylonite to metasomatic rocks along the Sashu Fault, SW Japan. Journal of Structural Geology 32, 792–802.
Sumino, H., Burgess, R., Mizukami, T., Wallis, S.R., Holland, G., Ballentine, C.J., 2010. Seawater-derived noble gases and halogens preserved in exhumed mantle wedge peridotite. Earth and Planetary Science Letters 294, 163–172.
Ulmer, P., Trommsdorff, V., 1995. Serpentine stability to mantle depths and subduction-related Magmatism. Science 268, 858–861.
Wada, I., Wang, K., He, J., Hyndman, R.D., 2008. Weakening of the subduction interface and its effects on surface heat flow, slab dehydration, and mantle wedge serpentinization. Journal of Geophysical Research 113, B04402.
Wallis, S.R., Kobayashi, H., Nishii, A., Mizukami, T., Seto, Y., Obliteration of olivine crystallographic preferred orientation patterns in subduction-related antigorite-bearing mantle peridotite: an example from the Higashi-Akaishi body, SW Japan. In: Prior, D.J., Rutter, E.H., Tatham, D.J. (Eds.), Deformation Mechanism, Rheology & Tectonics: Microstructures, Mechanics & Anisotropy – The Martin Casey Volume. Geological Society of London, Special Publication, in press.
Woodcock, N.H., 1977. Specification of fabric shapes using an eigenvalue method. Geological Society of America Bulletin 88, 1231–1236.
Woodcock, N.H., Naylor, M.A., 1983. Randomness testing in three-dimensional orientation data. Journal of Structural Geology 5, 539–548.